Inorganic Chemistry

pubs.acs.org/IC

Article

Flux Growth of Cerium Nickel Gallides Studied by In Situ Neutron Diffraction

Jo W. Haddock, Zach J. Barton, Keke Feng, Ryan E. Baumbach, Qiang Zhang, and Susan E. Latturner*

Cite This: https://doi.org/10.1021/acs.inorgchem.2c02588

Read Online

ACCESS | Metrics & More | Article Recommendations | Supporting Information

ABSTRACT: Reactions of cerium and nickel in excess molten gallium were monitored by neutron diffraction during heating and cooling. The formation of binary intermediates $CeGa_2$ and Ni_2Ga_3 was observed during heating. During cooling of the molten mixture from 900 °C, precipitation of $BaAl_4$-type $CeNi_{0.74}Ga_{3.26}$ occurred at 850 °C. Upon cooling to 650 °C, this compound reacted in the flux to form Ce_2NiGa_{10} and then Ce_2NiGa_{12}, the latter of which persisted to room temperature. Making use of this information, subsequent reactions were quenched at 750 °C to isolate crystals of $CeNi_{0.74}Ga_{3.26}$ for further study. Similar reactions replacing Ce with La and quenching above 750 °C yielded $LaNi_{0.35}Ga_{3.65}$ crystals. Magnetic susceptibility studies on $CeNi_{0.74}Ga_{3.26}$ indicate that the cerium is trivalent; the Ce^{3+} moments undergo a strongly anisotropic ferromagnetic ordering with moment perpendicular to the *c* axis below 7 K. Heat capacity data show little evidence of heavy fermion behavior. Resistivity measurements show that both $LaNi_{0.35}Ga_{3.65}$ and $CeNi_{0.74}Ga_{3.26}$ exhibit metallic behavior. Density of states calculations support this and indicate that Ni/Ga mixing in the compound stabilizes the structure.

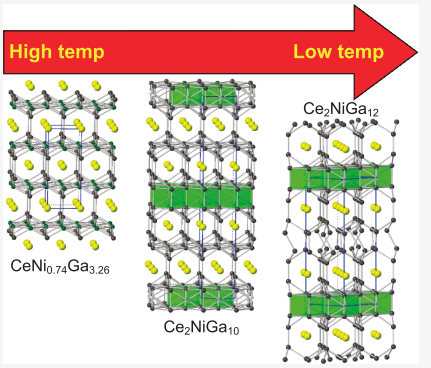

INTRODUCTION

Metal fluxes are useful media for exploratory synthesis of intermetallics and Zintl phases and for growth of large single crystals for physical property measurements. Metal flux reactions make use of a large excess of a low melting metal that dissolves the other reactants; this solution-based method eliminates diffusion barriers common in solid-state synthesis techniques and allows good crystal growth of products.[1−3] Metals commonly used as solvents in flux synthesis include tin, aluminum, indium, and gallium. Gallium is particularly attractive due to its low melting point and high boiling point, allowing for a wide reaction temperature range. Intermetallic compounds grown from gallium flux include Sm_2NiGa_{12}, Ho_2CoGa_8, Ce_2NiGa_{12}, $CePd_{3+x}Ga_{8-x}$, $Ba_8Ga_{16}Ge_{30}$, and $EuGa_2As_2$.[4−9]

The formation of multiple competing phases with no information about reaction mechanism (and thus little ability to predict and control reaction outcome) is one of the issues that is encountered in using this technique. Flux reactions are typically carried out in sealed ampules inside furnaces at high temperatures, making the detection of intermediate phases very difficult. Altering reaction parameters (reactant ratio, heating rate, maximum temperature, cooling rate, quench temperature) can result in the formation of different intermediate phases and final products. The usual way to optimize flux syntheses is to run multiple reactions and vary one parameter at a time. This process can be streamlined using in situ diffraction experiments, wherein a flux reaction is carried out in a heated sample holder in a diffractometer to enable the observation of phase transformation events as the temperature is changed. This technique allows for the detection of intermediate phases that may form and interconvert during heating or cooling of a reaction mixture. The use of in situ diffraction has been demonstrated for syntheses of complex metal sulfides in polysulfide salt fluxes by Kanatzidis et al.[10] It has also been used by the O'Hare and zur Loye groups to study the growth of oxides in Na_2SO_4 and KCl/NaCl fluxes.[11,12] There have been few reports on similar experiments to explore metal flux reactions due to problems such as high absorbance and attack on reaction ampules by molten metals.[13] The Latturner group used in situ neutron diffraction to investigate reactions of barium, ytterbium, and silicon in Mg/Al flux, a system that yielded four Ba/Yb/Mg/Si products and is highly sensitive to slight perturbations in the cooling profile.[14]

In this work, we used in situ neutron diffraction to study the reaction of cerium and nickel in excess gallium flux. The low melting point of gallium and its lack of reactivity toward silica tubing make it ideal for in situ studies to help identify intermediates formed during the reaction and shed light on the

Received: July 20, 2022

mechanism of reaction. The Ce/Ni/Ga system is of interest due to the plethora of known ternary phases, which include Ce_2NiGa_{12},[6] Ce_4NiGa_{18},[15] $CeNiGa_6$,[16] Ce_2NiGa_{10},[17] $Ce_3Ni_2Ga_{15}$,[18] and $Ce(Ni/Ga)_4$ (two forms).[19,20] All of these compounds have structures comprised of $BaAl_4$-type cerium gallide slabs separated by antifluorite-type $NiGa_2$ layers. Several identical Ce/Ni/Ga reactions were prepared, and different cooling rates were explored. In all cases, $BaAl_4$-type $CeNi_{0.74}Ga_{3.26}$ is formed at high temperatures and converts into Ce_2NiGa_{10} and then Ce_2NiGa_{12} as the reaction cools below 550 °C. This reaction was reproduced in the lab and quenched at high temperatures, enabling the isolation of large crystals of $CeNi_{0.74}Ga_{3.26}$; a similar reaction using lanthanum yielded $LaNi_{0.35}Ga_{3.65}$ crystals. Magnetic characterization indicates that $CeNi_{0.74}Ga_{3.26}$ contains trivalent cerium and undergoes ferromagnetic ordering below 7 K.

EXPERIMENTAL PROCEDURE

Synthesis (Ex Situ Reactions). Ce chunks (Alfa-Aesar, 99.8%), Ni powder (Alfa-Aesar, 99.8%), and Ga chips (Alfa-Aesar, 99.9%) were combined in a 2:1:20 mmol ratio in a silica ampule (7 mm ID, 9 mm OD). Silica wool was placed above the reactants to act as a filter during centrifugation. This silica ampule was then sealed under a vacuum at 100 mbar. Several reaction ampules were prepared, and a variety of heating profiles were explored in preliminary experiments using different maximum temperatures and cooling rates but all ending with centrifuging at 200 °C to remove the excess molten gallium flux. The crystals collected were rectangular plate shaped in appearance and were silver colored and reflective. After the neutron diffraction study (vide infra) that indicated the importance of centrifuge temperature, the temperature profile was altered with reactions being centrifuged at 800 to 600 °C at 50 °C intervals. Additionally, the rate of cooling from 1000 °C to the centrifuge temperature was slowed in an attempt to increase the size of the crystals.

To ensure that the temperature of the reaction did not drop significantly during centrifugation, the reaction vessel was prepared as described above. This silica ampule was then placed in a second larger ampule (11 mm ID, 13 mm OD) and sealed under a vacuum at 100 mTorr. This second vacuum jacket provides additional thermal insulation of the inner vessel during removal from the furnace and centrifugation.

Elemental Analysis. Products were analyzed by SEM-EDS using an FEI Nova 400 NanoSEM with energy dispersive spectroscopy (EDS) capabilities. Samples of product crystals were mounted onto aluminum pucks using double-sided carbon tape and analyzed using a 25 kV acceleration voltage. The surface of the pucks was completely covered with the carbon tape to eliminate artifacts produced by the aluminum. The surface of the crystals showed residual flux droplets in some areas, so measurements were taken on cleaved samples or on surfaces where no flux was present.

Single-Crystal X-ray Diffraction Studies. Samples were examined under a microscope to select crystals for diffraction studies. Suitable pieces were cut from larger crystals and were mounted in Dual-Thickness MicroLoops (MiTeGen Loop/Mount) using Parabar oil. Single-crystal X-ray diffraction data were collected at 200 K using a Rigaku XtaLAB Synergy-S diffractometer equipped with a HyPix-6000HE Hybrid Photon Counting (HPC) detector and dual Mo and Cu microfocus sealed X-ray source. Refinements of structures were performed with the SHELXTL package using the SHELXLe user interface.[21,22] The 4*d* and 4*e* sites of the RNi_xGa_{4-x} compounds ($BaAl_4$-type, space group *I*4/*mmm*) were initially assigned as fully occupied by gallium; then their occupancy was allowed to vary. The 4*d* site refined as 100% occupied, while the occupancy of the 4*e* site dropped, indicating the mixing of lighter Ni on this site. The 4*d* site was therefore fixed as fully occupied by Ga, and the 4*e* site refined as a Ni/Ga mixed site. The resulting stoichiometries matched the compositions indicated by SEM-EDS elemental analysis. Crystallographic data for $CeNi_{0.74}Ga_{3.26}$ and $LaNi_{0.35}Ga_{3.65}$ are found in the Supporting Information (Tables S1 and S2), and the CIF files are also available from the Cambridge Crystallographic Data Centre under deposition numbers 2189804 and 2189805.

Powder Neutron Diffraction Studies. Four identical samples were prepared for in situ neutron diffraction studies using the POWGEN diffractometer on beamline 11A at the ORNL Spallation Neutron Source.[23] Each reaction ampule contained 20 mmol of gallium, 1 mmol of nickel, and 2 mmol of cerium in a sealed silica tube that is 9 mm in outside diameter. The ampule was flame-sealed under a vacuum so that its length was less than 5 cm to fit into the vanadium sample holder for the MICAS furnace. To explore this system, the heating profile was altered for each sample.

- Sample 1: Data collection while heating up to 1000 °C in 2 h. Hold at 1000 °C for 1 h for long scan. Data collection while cooling to 200 °C with a slow rate of 1.6 C/m (in 8 h)
- Sample 2: Heat to 900 °C in 2 h, hold at 900 °C for 1 h, cool to 200 °C in 8 h
- Sample 3: Heat to 900 °C in 2 h, hold at 900 °C for 1 h, cool to 200 °C in 4 h
- Sample 4: Use a heating profile with three heating cycles: Heat from RT to 700 °C at 5°/min. Hold at 700 °C for 1 h. Cool to 200 °C in 10 °/min. Hold at 200 °C for 3 h. Heat from 200 to 900 °C at 5 °/min. Hold at 900 °C for 1 h. Cool to 200 °C in 10 °/min. Hold at 200 °C for 3 h. Heat from 200 to 900 °C at 5 °/min. Hold at 900 °C for 1 h. Cool to 200 °C in 6 °/min. Hold at 200 °C for 3 h.

For each sample, diffraction data were continuously collected throughout the heating, dwell, and cooling process using the time event mode data collection at SNS that allows postprocessing of the data as described in a previous report.[24]

Magnetic and Electronic Property Characterization. Magnetic susceptibility measurements were conducted on a single crystal of $CeNi_{0.74}Ga_{3.26}$ to characterize the valence state of cerium and to detect possible magnetic ordering. A single crystal (2 × 2 × 0.5 mm) was grown from a reaction of 2:1:20 mmol ratio of Ce/Ni/Ga in the double-jacketed ampule configuration. This reaction was heated to 1000 °C in 5 h, held for 5 h, and then cooled to 750 °C in 72 h followed by centrifugation at 750 °C. The plate-shaped crystal was aligned on a piece of Kapton tape to position the short axis of the crystal (crystallographic *c* axis) perpendicular to the applied field. This tape was then placed in a straw and then attached to the sample rod of a Quantum Design MPMS SQUID system. Magnetic susceptibility $\chi = M/H$ data were collected from 1.8 to 300 K under an applied magnetic field of $H = 0.050$ T. Magnetization data were collected at $T = 1.8$ K, with measurements taken as the field was ramped from 7 to −7 T. The crystal was then repositioned to orient the *c* axis parallel to the applied field, and the data were collected in this configuration.

Electrical resistivity measurements for $T = 1.8-300$ K were performed in a four-wire configuration using a Quantum Design Physical Property Measurement System. Platinum wires were spot-welded in place on the sample for this measurement and were positioned so that the electrical current runs along the *ab*-plane of the crystal. Temperature-dependent heat capacity measurements were performed from 1.8 to 300 K using the thermal relaxation technique. Identical magnetic and electronic properties measurements were carried out on a single crystal of $LaNi_{0.35}Ga_{3.65}$ prepared using a similar flux growth technique (La/Ni/Ga ratio of 2:1:20 mmol).

Electronic Structure Calculations. Calculations were carried out on two models ($LaNi_2Ga_2$ and $LaGa_4$). Density of states (DOS) calculations were performed using the tight-binding linear muffin tin orbitals-atomic sphere approximation, which is implemented in the Stuttgart TB-LMTO-ASA software package (version 47.1b).[25,26] The structural model was based on unit cell parameters and atomic coordinates experimentally determined by single-crystal X-ray diffraction at 200 K for $CeNi_{0.74}Ga_{3.24}$. The TB-LMTO-ASA method is known to exhibit difficulties in convergence for model systems with lanthanide and actinide atoms that contain partially filled *f*-shells. Therefore, Ce atoms were modeled as La. In $CeNi_{0.74}Ga_{3.24}$, the Ga/

https://doi.org/10.1021/acs.inorgchem.2c02588
Inorg. Chem. XXXX, XXX, XXX−XXX

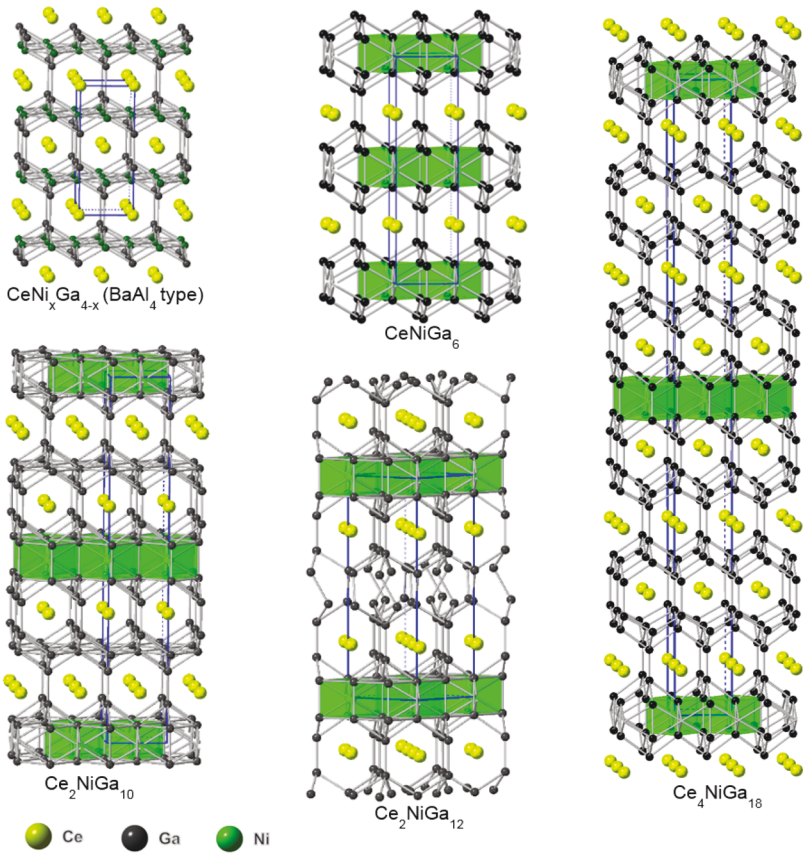

Figure 1. Structures of Ce/Ni/Ga intermetallic compounds. The antifluorite type $NiGa_2$ slabs are shown in polyhedral mode. (a) $CeNi_{0.74}Ga_{3.26}$ (*I*4/*mmm*, $ThCr_2Si_2$ type), (b) $CeNiGa_6$ (*P*4/*mmm*), (c) Ce_2NiGa_{10} (*I*4/*mmm*), (d) Ce_2NiGa_{12} (*P*4/*nbm*), and (e) Ce_4NiGa_{18} (*I*4/*mmm*).

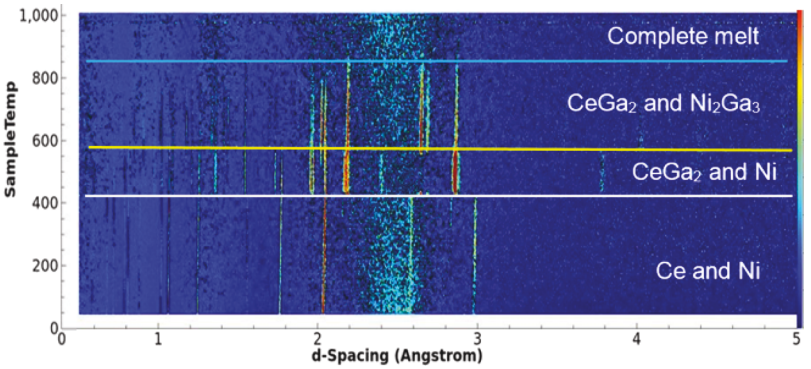

Figure 2. Neutron diffraction data collected on a Ce/Ni/Ge reaction (2:1:20 mmol ratio) as it is heated up to 1000 °C in 2 h. Transition temperatures are highlighted by horizontal lines.

Ni mixed site is ∼47% occupied by Ga and ∼53% by Ni. Two test models were calculated: one treating this site as fully occupied by Ga and the other treating this site as fully occupied by Ni. The overall stoichiometries of the model phases were therefore $LaNi_2Ga_2$ ("Ni-rich model") and $LaGa_4$ ("Ga-rich model").

RESULTS AND DISCUSSION

The Ce/Ni/Ga system has been explored by several research groups due to the extensive family of related structures that arises from combinations of these elements. In particular, Grin et al. explored the ternary phase diagram using arc melting of stoichiometric mixtures, reporting a homologous series of compounds containing $BaAl_4$-type Ce/Ga slabs of varying thicknesses separated by antifluorite-type $NiGa_2$ layers.[15−18] As a result of these structural building blocks, all the compounds are either tetragonal or a slight distortion thereof (leading to orthorhombic symmetry). This series includes $CeNiGa_3$ (either $ThCr_2Si_2$-type in *I*4/*mmm* or $CePtGa_3$-type in *Fmm*2),[19,20] $CeNiGa_6$ (*P*4/*mmm*),[16] Ce_2NiGa_{10} (*I*4/*mmm*),[17] Ce_2NiGa_{12} (*P*4/*nbm*),[6] and Ce_4NiGa_{18} (*I*4/*mmm*),[15] some of which are shown in Figure 1. In addition to their structural complexity, the electronic/magnetic properties of these materials are also of interest due to the unique behaviors that can occur in cerium intermetallics such as mixed or fluctuating valency, the Kondo effect, and superconductivity.[27−30] Our preliminary investigations of reactions of cerium and nickel in excess gallium flux, typically quenched by centrifuging at temperatures around 200 °C, yielded predominantly Ce_2NiGa_{12}, a compound that has already

https://doi.org/10.1021/acs.inorgchem.2c02588
Inorg. Chem. XXXX, XXX, XXX−XXX

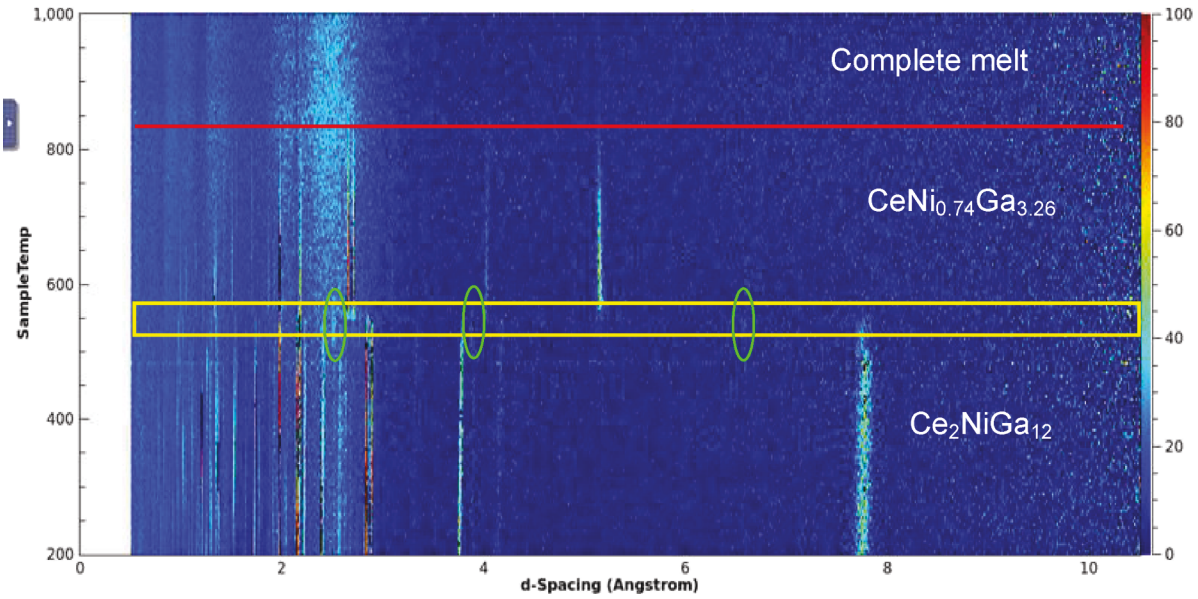

Figure 3. Neutron diffraction data collected on a Ce/Ni/Ge reaction (2:1:20 mmol ratio) as it is cooled from 1000 °C at a rate of 1.6 °C/min (in 8 h). Transition temperatures are highlighted by horizontal lines.

Table 1. SEM-EDS Elemental Analysis Data and Unit Cell Parameters Determined by SC-XRD for Products of Ce/Ni/Ga Flux Reactions in 2:1:20 mmol Ratios Centrifuged at Different Temperatures

centrifuge temp (°C)	mol % cerium	mol % nickel	mol % gallium	*a* (Å)	*c* (Å)	space group	structure
800	20.1(7)	7.0(3)	72.8(4)	4.3157(2)	10.2648(8)	*I*4/*mmm*	$CeNi_{0.74}Ga_{3.26}$
750	20.6(3)	7.0(7)	72.3(2)	4.3157(8)	10.3093(5)	*I*4/*mmm*	$CeNi_{0.74}Ga_{3.26}$
700	20.4(8)	7.0(6)	72.4(8)	4.3174(1)	10.3520(6)	*I*4/*mmm*	$CeNi_{0.74}Ga_{3.26}$
650	19.3(5)	7.0(3)	73.6(1)	4.3182(2)	10.3137(7)	*I*4/*mmm*	$CeNi_{0.74}Ga_{3.26}$
600	27.4(2)	7.7(5)	64.8(4)	4.2568(1)	26.358(1)	*I*4/*mmm*	Ce_2NiGa_{10}
550	23.8(5)	5.5(7)	70.5(6)	6.0239(1)	15.4842(4)	*P*4/*nbm*	Ce_2NiGa_{12}
500	23.6(6)	5.8(6)	70.6(8)	6.0300(2)	15.4739(8)	*P*4/*nbm*	Ce_2NiGa_{12}
450	24.1(4)	5.4(2)	70.5(5)	6.0262(1)	15.4758(4)	*P*4/*nbm*	Ce_2NiGa_{12}
400	23.7(3)	5.1(6)	71.2(4)	6.0264(1)	15.4733(5)	*P*4/*nbm*	Ce_2NiGa_{12}

been well-characterized.[6] Gallium acts as a reactive flux, incorporating into the products that form. In situ neutron diffraction studies were carried out to determine if other phases form at high temperatures or with different cooling rates.

In Situ Neutron Diffraction Study. In situ neutron diffraction studies were carried out on four samples of identical stoichiometry (Ce/Ni/Ga in 2:1:20 mmol ratio). Data collected during heating are shown in Figure 2. Diffraction peaks corresponding to cerium and nickel metal reactants are observed until reaching a temperature of 420 °C; at this point, the cerium metal reacts with the gallium flux to form $CeGa_2$. As the temperature rises above 570 °C, the nickel metal reacts to form Ni_2Ga_3. All diffraction peaks disappear above 860 °C, indicating the dissolution of all solids into the gallium melt.

Cooling this molten mixture leads to the precipitation of $ThNi_2Si_2$-type $CeNi_{0.74}Ga_{3.26}$ at 830 °C. This compound is maintained as the reaction mixture cools to 600 °C, at which point it transforms into Ce_2NiGa_{12}. The presence of a transition phase between 550 and 600 °C is indicated by a few faint diffraction peaks that appear and disappear (see Figure 3). These temperatures and transformations were reproducible in all four samples that were run, regardless of changing of cooling rates and maximum temperatures. One of the reactions was reheated to 900 °C after being cooled to 200 °C; because a complete melt was obtained above 860 °C, the sequence and temperatures of precipitation of the two products were again reproduced. Structural refinements based on the in situ data were not possible due to effects of the preferred orientation; crystal growth occurs along favored directions in the reaction ampules.

Ex Situ Reactions and Structures. Based on the results of the in situ neutron diffraction study, the product in this reaction system is dependent on the temperature. $CeNi_{0.74}Ga_{3.26}$ precipitates at high temperatures and converts to Ce_2NiGa_{12} in the molten flux as the reaction cools below 550–600 °C. To enable the isolation and study of the high-temperature $CeNi_{0.74}Ga_{3.26}$ phase, we focused our ex situ efforts on centrifuging reactions in the temperature range at and above 600 °C (results shown in Table 1). One of the inherent difficulties in ex situ studies is the cooling of the reaction as it is removed from the furnace; if the tube cools below the transition temperature before removal of the flux in the centrifuge, Ce_2NiGa_{12} is isolated. This problem was solved by placing the reaction ampule inside another vacuum-sealed silica jacket to provide thermal insulation during the centrifugation process. The initial $CeNi_{0.74}Ga_{3.26}$ crystals isolated were very small; this was remedied by slowing the cooling rate (from 1000 to 750 °C in 72 h; centrifuging at 750 °C). This produced much larger crystals.

https://doi.org/10.1021/acs.inorgchem.2c02588
Inorg. Chem. XXXX, XXX, XXX−XXX

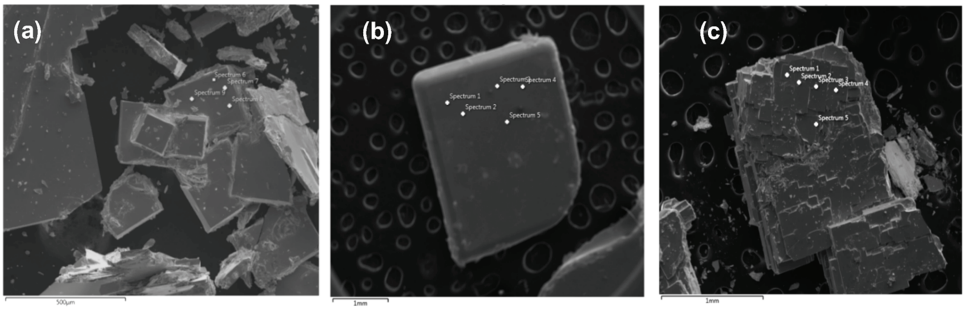

Figure 4. SEM images of crystals isolated from a Ce/Ni/Ga flux reaction (with a 2:1:20 mmol ratio). (a) Ce_2NiGa_{12} crystals formed from the reaction centrifuged at 600 °C. (b) $CeNi_{0.74}Ga_{3.26}$ crystals formed from the reaction centrifuged at 800 °C. (c) Mixed phases from the reaction centrifuged at 650 °C.

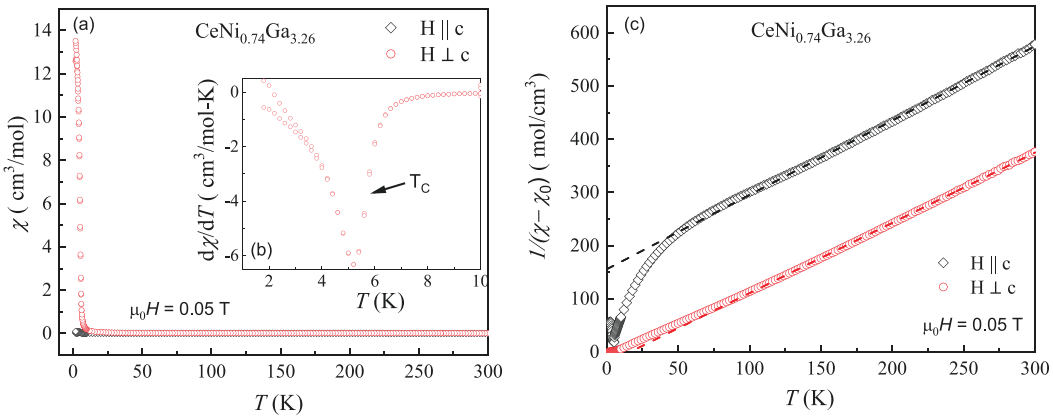

Figure 5. (a) Magnetic susceptibility data ($\chi = M/H$) for a crystal of $CeNi_{0.74}Ga_{3.26}$ oriented with the c axis parallel (black open diamond) and perpendicular (red open circle) to the applied field of $\mu_0 H = 0.05$ T. Inset (b) plots the derivatives of the magnetic susceptibilities with respect to temperature. Black arrow indicates the T_C at 5.5 K. (c) The inverse magnetic susceptibility $\chi^{-1} = (M/H)^{-1}$ vs temperature T oriented with the c axis parallel (black open diamond) and perpendicular (red open circle) to the applied field of $\mu_0 H = 0.05$ T. The dotted line is a fit to the data using the modified Curie−Weiss law, as described in the text.

Centrifuging of a reaction at 600 °C yielded mostly $CeNi_{0.74}Ga_{3.26}$, but a few crystals of Ce_2NiGa_{10} were also isolated in the product mixture. The presence and low yield of this phase may indicate that it is formed during the transformation of $CeNi_{0.74}Ga_{3.26}$ into Ce_2NiGa_{12} during cooling. In the in situ neutron diffraction data, a few faint diffraction peaks appear and disappear as the temperature cools from 600 to 500 °C (see Figure 3). These peaks are consistent with the calculated pattern for Ce_2NiGa_{10} (the peak at d-spacing of 2.5 Å corresponding to the (019) reflections, the peak at 3.8 Å to the (013) reflections, and the peak at 6.6 Å to the (004) reflections). Roughly doubling the formula of $CeNi_{0.74}Ga_{3.26}$ to "Ce_2NiGa_7", the transformation during cooling of this flux reaction is thus $Ce_2NiGa_7 \rightarrow Ce_2NiGa_{10} \rightarrow Ce_2NiGa_{12}$. This indicates the intercalation of gallium from the flux into the cooling structure as the nickel position becomes more ordered, moving into the antifluorite $NiGa_2$ slabs that further separate as more gallium enters the structure.

Single-Crystal X-ray Diffraction Studies. Flux-grown $CeNi_{0.74}Ga_{3.26}$, Ce_2NiGa_{12}, and Ce_2NiGa_{10} appear similar under the microscope, all forming as silver rectangular plates. Images of $CeNi_{0.74}Ga_{3.26}$ and Ce_2NiGa_{12} are shown in Figure 4a,b. It was not possible to isolate the intermediate Ce_2NiGa_{10} as a pure phase. Crystals of this compound were occasionally obtained from reactions centrifuged at or near 600 °C, mixed with crystals of the other Ce/Ni/Ga phases; the poor quality of the transforming crystals is evident in their fragmented appearance (Figure 4c). Elemental analyses from EDS data of a sample centrifuged at 800 °C show 20.16(4) mol % Ce, 7.02(2) mol % Ni, and 72.83(1) mol % Ga, supporting a stoichiometry of $CeNi_{0.74}Ga_{3.26}$. Similar analysis of crystals isolated from centrifuging a reaction at 500 °C yielded values of 23.86 mol % Ce, 5.58 mol % Ni, and 70.56 mol % Ga, consistent with the Ce_2NiGa_{12} structure; see Table 1.

Single-crystal X-ray diffraction data on crystals isolated from reactions centrifuged below 500 °C were in agreement with the previously reported Ce_2NiGa_{12} structure.[6] This forms in the tetragonal space group $P4/nbm$ (see Figure 1). Centrifuging above the transition temperature yields crystals of $BaAl_4$-type $CeNi_xGa_{4-x}$ in tetragonal space group $I4/mmm$. Refinement of SC-XRD data indicates that nickel and gallium mix on the 4e Wyckoff site (37.6 and 62.4% respective occupancy). The 4d site is occupied only by gallium. The resulting stoichiometry is $CeNi_{0.74}Ga_{3.26}$. This stoichiometry was consistently observed in all crystals that were centrifuged at various temperatures above 650 °C (analyzed by EDS and SC-XRD), indicating that the Ni/Ga ratio in the precipitated phase is constant. The Ni/Ga siting observed for our flux-grown samples is different from that reported by Cava et al. for $CeNiGa_3$; they observed Ni/Ga mixing in 25/75% amounts on both 4d and 4e sites.[19] On the other hand, our results support the hypothesis given by Grin et al. in their 1990 report on $CeNi_xGa_{4-x}$; based on the dependence of unit cell parameters on x and analogies to isostructural $CePd_xGa_{4-x}$, they assumed that Ni preferentially

https://doi.org/10.1021/acs.inorgchem.2c02588
Inorg. Chem. XXXX, XXX, XXX−XXX

mixed on the 4*e* site, although Ni/Ga mixing could not be refined at the time.[20] Similarly, our flux reactions with lanthanum (La/Ni/Ga, 2:1:20 mmol ratio) centrifuged above 750 °C produced $LaNi_{0.35}Ga_{3.65}$, with Ni/Ga mixing on the 4*e* Wyckoff site and only gallium found on the 4*d* Wyckoff position. SEM-EDS elemental analysis data indicated values of 20.0(2) mol % La, 5.32(7) mol % Ni, and 74.7(3) mol % Ga, which correspond to a stoichiometry slightly richer in gallium ($LaNi_{0.3}Ga_{3.7}$) than the SC-XRD refinement. It is notable that $BaAl_4$-type binary phases $LaGa_4$ and $CeGa_4$ have not been reported; some nickel incorporation appears necessary to stabilize the structure.

Magnetic Susceptibility. As summarized in Figure 5, temperature-dependent magnetic susceptibility $\chi(T)$ data were collected for $LaNi_{0.35}Ga_{3.65}$ and $CeNi_{0.74}Ga_{3.26}$ single crystals with the magnetic field of 0.05 T applied parallel and perpendicular to the crystallographic *c* axis. The lanthanum analog shows temperature-independent behavior that is weakly diamagnetic (data shown in the Supporting information, Figure S1). This is likely due to a combination of weak Pauli paramagnetism from the conduction electrons combined with the core diamagnetism. In contrast, the cerium compound shows Curie−Weiss paramagnetic behavior at high temperatures, consistent with the cerium ions being in a trivalent state. Easy *ab*-plane anisotropy is observed, with a sharp rise in χ near T_C = 5.6 K indicating ferromagnetic ordering. This is a higher ordering temperature than what is seen in other $CeNi_xGa_{4-x}$ analogs ($CeNiGa_3$ and $CeNi_{0.5}Ga_{3.5}$ show T_C values of 2 and 5 K, respectively), showing that the Ni/Ga ratio tunes the magnetic behavior.[19,20] For $T < T_C$, $\chi(T)$ for *H* applied perpendicular to the *c* axis is significantly higher than in the parallel orientation, consistent with the moments aligning in the *ab*-plane in the ordered state. This is in contrast to many Kondo lattice ferromagnets that order along the magnetically hard direction of the Kramers doublet.[31] Instead, it resembles what is seen for the local moment ferromagnet $CePd_2P_2$, where the paramagnetic easy axis is the same as the ordered state easy axis.[32]

Further insight is gained from fits to the high-temperature data (100 K ≤ *T* ≤ 300 K) using a modified Curie−Weiss law ($\chi = [C/(T-\theta)] + \chi_0$) as seen in Figure 5c. The fits yield very small values of χ_0 = −0.00069 and 0 emu/mol for *H* applied parallel and perpendicular to the crystallographic *ab*-plane, consistent with the small diamagnetic signal of the lanthanum analog (Figure S1). Large differences in the Curie−Weiss constant are also observed (θ = −111 and 16.3 K for *H* parallel and perpendicular to *c*, respectively), reflecting the anisotropy of the magnetic coupling. The magnetic moment per cerium ion, calculated from Curie constant *C*, is similar in both orientations (μ_{eff} = 2.39 and 2.46 μ_B/f.u. for parallel and perpendicular orientations, respectively) and is in agreement with the expected value of 2.54 μ_B for trivalent cerium. Finally, at temperatures below 50 K, there is a deviation from the Curie−Weiss behavior due to crystal electric field splitting of the Hund's rule multiplet.

Magnetization data collected for $CeNi_{0.74}Ga_{3.26}$ at 1.8 K (below the ordering temperature) also reveal ferromagnetic order with strong anisotropy (Figure 6). The data collected with the field perpendicular to the *c* axis clearly show a saturation of the magnetization above 0.5 T, with an M_{sat} of 1.5 μ_B per formula unit. This value resembles what is seen for other Ce-based ferromagnets with crystal electric field split ground states.[32,33] The lack of hysteresis indicates soft ferromagnetism. There is no clear saturation for the data collected with the field parallel to the *c* axis, although there is a subtle increase in *M* at large fields that may indicate the onset of a metamagnetic phase transition.

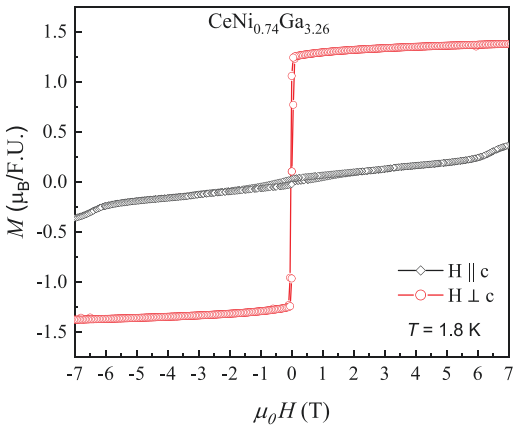

Figure 6. Magnetization data collected at 1.8 K for a single crystal of $CeNi_{0.74}Ga_{3.26}$ oriented with the *c* axis parallel and perpendicular to the applied field.

Electronic Properties. Temperature-dependent heat capacity $C(T)$ data for $LaNi_{0.35}Ga_{3.65}$ and $CeNi_{0.74}Ga_{3.26}$ single crystals are shown in Figure 7a. At elevated temperatures, both compounds exhibit similar behavior, reflecting comparable lattice contributions. Near 10 K, C/T for the Ce-analogue deviates from the lattice behavior by gradually increasing with decreasing *T* due to the onset of magnetic fluctuations that precede the magnetic ordering seen in $\chi(T)$ at T_C = 5.6 K. C/T subsequently drops to smaller values but only reaches 0.56 J/mol·K^2 at 1.8 K, indicating a substantial residual magnetic heat capacity that obscures the electronic component of the heat capacity expressed by the Sommerfeld coefficient γ. To overcome this, we use the expression $C/T = \gamma + \beta T^2$ to fit the data for $CeNi_{0.74}Ga_{3.26}$ in the temperature range of 13.2 K < *T* < 20.0 K, from which we find γ = 32.1 mJ/mol·K^2. This is compared to the value γ = 3.77 mJ/mol·K^2 for the lanthanum analogue (fitting the data from 1.8 to 7.0 K). The Sommerfeld coefficient γ is proportional to the charge carrier effective mass and is often enhanced in "heavy fermion" cerium-based materials where there is strong hybridization between the *f*- and conduction electron states. The γ value of 32.1 mJ/mol·K^2 for $CeNi_{0.74}Ga_{3.26}$ shows that the effective mass of its charge carriers is slightly higher than that of the La analog. These fits also yield the values β = 0.92 mJ/mol·K^4 for $CeNi_{0.74}Ga_{3.26}$ and 0.44 mJ/mol·K^4 for $LaNi_{0.35}Ga_{3.65}$, which are used to calculate the respective Debye temperatures $\theta_D = \left(\frac{12\pi^4 R}{5\beta}\right)^{1/3}$ = 128.2 and 164.0 K. However, note that the La analogue only saturates toward a quadratic temperature dependence below *T* = 10 K. This suggests that the fits for the Ce compound above this range are not completely in the low temperature limit of the Debye function, which leads to some uncertainty in the value of γ. It is nonetheless clear that γ is enhanced by comparison to the La analogue as seen in the offset between the C/T curves at temperatures above 10 K, consistent with there being marginal Kondo lattice hybridization.

Further insight is gained from the electrical resistivity measurements (Figure 7b), which reveal metallic behavior for both compounds. Both analogs have RRR values (ρ_{300K}/ρ_{10K}) of 1.3−1.4, likely due to the inherent disorder in the structure

https://doi.org/10.1021/acs.inorgchem.2c02588
Inorg. Chem. XXXX, XXX, XXX−XXX

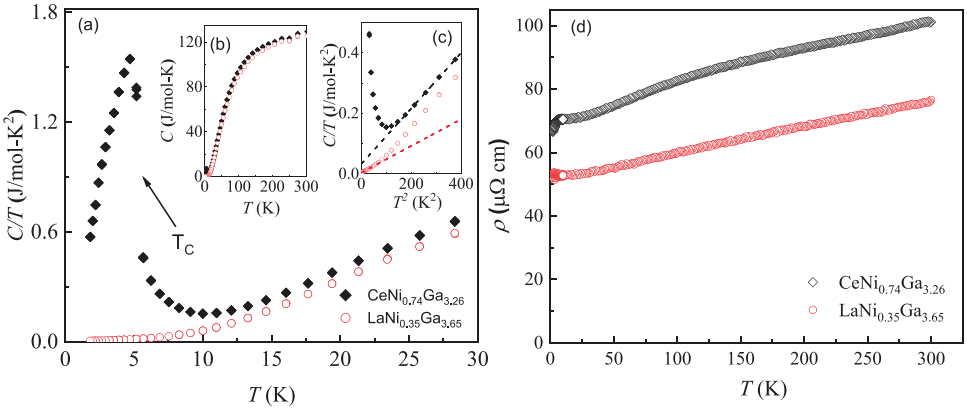

Figure 7. (a) Temperature-dependent heat capacity for $LaNi_{0.35}Ga_{3.65}$ and $CeNi_{0.74}Ga_{3.26}$ at low temperatures below 30 K. The black arrow indicates the transition temperature T_C at 5.62 K. Inset (b) shows heat capacity C vs temperature T data in the temperature range from 1.8 to 300 K. Inset (c) shows C/T vs T^2 data at low temperatures with solid lines representing the $C/T = \gamma + \beta T^2$ relation as described in the text. (d) Electrical resistivity data for $LaNi_{0.35}Ga_{3.65}$ and $CeNi_{0.74}Ga_{3.26}$.

caused by Ni/Ga mixing on the 4*e* Wyckoff site. We additionally note that the temperature dependence for $CeNi_{0.74}Ga_{3.26}$ exhibits curvature at elevated temperatures that is associated with the interactions between the conduction electrons and the *f*-states. The electrical resistivity of this compound also decreases abruptly near T_C due to the removal of spin disorder scattering.

Electronic Structure Calculations. To investigate the effects of Ni/Ga mixing in the structure, density of states (DOS) calculations were carried out on two models: $LaNi_2Ga_2$ and $LaGa_4$. Both models are based on the structural data collected for $CeNi_{0.74}Ga_{3.24}$, with the mixed occupancy 4*e* Wyckoff site modeled as fully occupied by either nickel (yielding $LaNi_2Ga_2$) or gallium (yielding $LaGa_4$). As seen in Figure 8, both models have a nonzero DOS at the Fermi level,

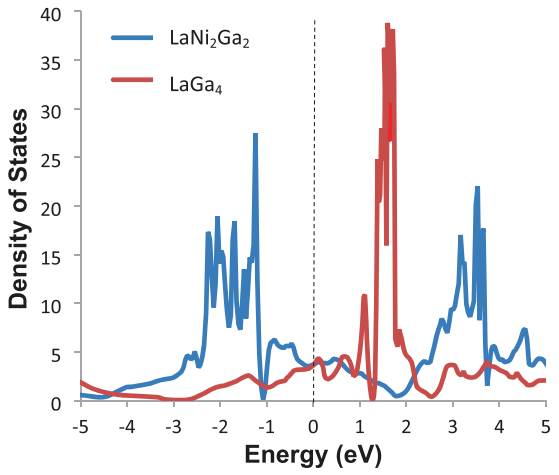

Figure 8. Density of states diagrams of the nickel-rich $LaNi_2Ga_2$ (blue line) and the gallium-rich $LaGa_4$ (red line) models. Fermi level indicated by the dashed line at 0 eV.

in agreement with their metallic character. A narrow cluster of 4*f*-bands from the La^{3+} ions is positioned above the Fermi level (centered at 1.6 and 3.1 eV for $LaGa_4$ and $LaNi_2Ga_2$, respectively). The $LaNi_2Ga_2$ model features bands derived from nickel 3*d*-orbitals from −1 to −3 eV below E_F. These bands are filled; therefore, nickel does not contribute to the magnetism of the compound.

The actual compound $CeNi_{0.74}Ga_{3.26}$ has a different electron count, intermediate between the two models but closest to the $LaGa_4$ model. The density of states for $LaGa_4$ has a pseudogap below the Fermi level at −1 eV. Replacing Ga in the structure with Ni reduces the overall number of electrons, potentially shifting E_F into this pseudogap. Similarly, the $LaNi_2Ga_2$ model has a pseudogap at around 2 eV above the Fermi level. Replacing some of the nickel with gallium may act to shift the Fermi level into this pseudogap. This points to the stabilizing effect of Ni/Ga mixing in this compound; positioning E_F in a pseudogap tends to stabilize intermetallic compounds.

CONCLUSIONS

In situ neutron diffraction data provide crucial information for the discovery and isolation of compounds that form at high temperatures, as exemplified by the crystal growth of $CeNi_{0.74}Ga_{3.26}$ and $LaNi_{0.35}Ga_{3.22}$ in gallium flux reactions. It is notable that as the reaction is cooled, the products interconvert to form structures that incorporate more of the flux element. The ability to isolate the cerium analog as large crystals enabled the study of its strongly anisotropic ferromagnetic ordering. Further experimentation with this system will be conducted to determine if different ratios of elements could produce different nickel contents and sitings in the $CeNi_xGa_{4-x}$ structure or whether a different structure becomes favored. The disparity in the value of *x* for the cerium and lanthanum analogs is also of interest; from the reactant ratios, a 2:1 R/Ni incorporation (leading to a stoichiometry of $RNi_{0.5}Ga_{3.5}$) would be expected for both. The observed differences may indicate a potential size effect or possibly a slower equilibrium for one of the systems. If the latter is the case, modifying the cooling rate or adding an annealing step may enable the system to reach equilibrium and form products with the expected stoichiometry.

ASSOCIATED CONTENT

Supporting Information

The Supporting Information is available free of charge at https://pubs.acs.org/doi/10.1021/acs.inorgchem.2c02588.

Magnetic susceptibility data for $LaNi_{0.35}Ga_{3.65}$ (Figure S1); crystallographic information for $CeNi_{0.74}Ga_{3.26}$ (Table S1); and crystallographic information for $LaNi_{0.35}Ga_{3.65}$ (Table S2) (PDF)

https://doi.org/10.1021/acs.inorgchem.2c02588
Inorg. Chem. XXXX, XXX, XXX−XXX

Accession Codes

CCDC 2189804−2189805 contain the supplementary crystallographic data for this paper. These data can be obtained free of charge via www.ccdc.cam.ac.uk/data_request/cif, or by emailing data_request@ccdc.cam.ac.uk, or by contacting The Cambridge Crystallographic Data Centre, 12 Union Road, Cambridge CB2 1EZ, UK; fax: +44 1223 336033.

AUTHOR INFORMATION

Corresponding Author

Susan E. Latturner − *Department of Chemistry and Biochemistry, Florida State University, Tallahassee, Florida 32306, United States;* orcid.org/0000-0002-6146-5333; Email: jhaddock@fsu.edu

Authors

Jo W. Haddock − *Department of Chemistry and Biochemistry, Florida State University, Tallahassee, Florida 32306, United States*

Zach J. Barton − *Department of Chemistry and Biochemistry, Florida State University, Tallahassee, Florida 32306, United States*

Keke Feng − *FSU Department of Physics and National High Magnetic Field Laboratory, Tallahassee, Florida 32306, United States*

Ryan E. Baumbach − *FSU Department of Physics and National High Magnetic Field Laboratory, Tallahassee, Florida 32306, United States*

Qiang Zhang − *Neutron Scattering Division, Oak Ridge National Laboratory, Oak Ridge, Tennessee 37831, United States;* orcid.org/0000-0003-0389-7039

Complete contact information is available at: https://pubs.acs.org/10.1021/acs.inorgchem.2c02588

Notes

The authors declare no competing financial interest.

ACKNOWLEDGMENTS

This research was supported by the Division of Materials Research of the National Science Foundation (DMR-18-08471 and DMR-21-26077). This work utilized the resources of the X-ray Characterization Center in the Department of Chemistry and Biochemistry at FSU (FSU075000XRAY). The scanning electron microscope equipment in the Biological Sciences Imaging Resource (BSIR) of the Florida State University Department of Biology was also used; we thank Dr. Eric Lochner for guidance with this instrument. Part of this work was performed at the National High Magnetic Field Laboratory (NHMFL), which is supported by National Science Foundation Cooperative Agreement DMR-1644779, the State of Florida, and the Department of Energy. A portion of this research used resources at the Spallation Neutron Source, a DOE Office of Science User Facility operated by Oak Ridge National Laboratory.

REFERENCES

(1) Kanatzidis, M. G.; Pöttgen, R.; Jeitschko, W. The Metal Flux: A Preparative Tool for the Exploration of Intermetallic Compounds. *Angew. Chem., Int. Ed.* **2005**, *44*, 6996−7023.

(2) Phelan, W. A.; Menard, M. C.; Kangas, M. J.; McCandless, G. T.; Drake, B. L.; Chan, J. Y. Adventures in Crystal Growth: Synthesis and Characterization of Single Crystals of Complex Intermetallic Compounds. *Chem. Mater.* **2012**, *24*, 409−420.

(3) Latturner, S. E. Clusters, Assemble: Growth of Intermetallic Compounds from Metal Flux Reactions. *Acc. Chem. Res.* **2018**, *51*, 40−48.

(4) Chen, X. Z.; Small, P.; Sportouch, M.; Zhuravleva, M.; Brazis, P.; Kannewurf, C. R.; Kanatzidis, M. G. Molten Ga as a Solvent for Exploratory Synthesis: The New Ternary Polygallide Sm_2NiGa_{12}. *Chem. Mater.* **2000**, *12*, 2520−2522.

(5) Adriano, C.; Mendonça-Ferreira, L.; Bittar, E. M.; Pagliuso, P. G. Crystal Structure and Low Temperature Physical Properties of Ho_2CoGa_8 intermetallic antiferromagnet. *J. Appl. Phys.* **2008**, *103*, 07B712.

(6) Cho, J. Y.; Millican, J. N.; Capan, C.; Sokolov, D. A.; Moldovan, M.; Karki, A. B.; Young, D. P.; Aronson, M. C.; Chan, J. Y. Crystal Growth, Structure, and Physical Properties of Ln_2MGa_{12} (Ln = La, Ce; M = Ni, Cu). *Chem. Mater.* **2008**, *20*, 6116−6123.

(7) Francisco, M. C.; Malliakas, C. D.; Macaluso, R. T.; Prestigiacomo, J.; Haldolaarachchige, N.; Adams, P. W.; Young, D. P.; Jia, Y.; Claus, H.; Gray, K. E.; Kanatzidis, M. G. Structure and Phase Transitions of $CePd_{3+x}Ga_{8-x}$: New Variants of the $BaHg_{11}$ Structure Type *J. Am. Chem. Soc.* **2012**, *134*, 12998−13009.

(8) Latturner, S. E.; Bryan, J. D.; Blake, N.; Metiu, H.; Stucky, G. D. Siting of Antimony Dopants and Gallium in $Ba_8Ga_{16}Ge_{30}$ Clathrates Grown from Gallium Flux. *Inorg. Chem.* **2002**, *41*, 3956−3961.

(9) Goforth, A. M.; Hope, H.; Condron, C. L.; Kauzlarich, S. M.; Jensen, N.; Klavins, P.; MaQuilon, S.; Fisk, Z. Magnetism and Negative Magnetoresistance of Two Magnetically Ordering, Rare-Earth-Containing Zintl phases with a New Structure Type: $EuGa_2Pn_2$ (Pn = P, As). *Chem. Mater.* **2009**, *21*, 4480−4489.

(10) Shoemaker, D. P.; Hu, Y.-J.; Chung, D. Y.; Halder, G. J.; Chupas, P. J.; Soderholm, L.; Mitchell, J. F.; Kanatzidis, M. G. In Situ Studies of a Platform for Metastable Inorganic Crystal Growth and Materials Discovery. *Proc. Natl. Acad. Sci.* **2014**, *111*, 10922−10927.

(11) Moorhouse, S. J.; Wu, Y.; Buckley, H. C.; O'Hare, D. Time-resolved in situ Powder X-ray Diffraction Reveals the Mechanisms of Molten Salt Synthesis. *Chem. Commun.* **2016**, *52*, 13865.

(12) Abeysinghe, D.; Huq, A.; Yeon, J.; Smith, M. D.; zur Loye, H. C. In Situ Neutron Diffraction Studies of the Flux Crystal Growth of the Reduced Molybdates $La_4Mo_2O_{11}$ and $Ce_4Mo_2O_{11}$: Revealing Unexpected Mixed-Valent Transient Intermediates and Determining the Sequence of Events during Crystal Growth. *Chem. Mater.* **2018**, *30*, 1187−1197.

(13) Weiland, A.; Frith, M. G.; Lapidus, S. H.; Chan, J. Y. In situ Methods for Metal-flux Synthesis in Inert Environments. *Chem. Mater.* **2021**, *33*, 7657−7664.

(14) Vasquez, G.; Huq, A.; Latturner, S. E. In situ Diffraction Studies of the Growth of Ba/Yb/Mg/Si Intermetallics in Mg/Al Flux. *Inorg. Chem.* **2019**, *58*, 8111−8119.

(15) Grin, Y.; Yarmolyuk, Y. P.; Usov, O. A.; Kuz'min, A. M.; Bruskov, V. A. The Crystal Chemistry of a Series of Inhomogeneous Structures. The Crystal Structure of the Compounds $Ce_4Ga_{17}Ni_2$ and $Nd_4Ga_{17}Ni_2$. *Kristallografiya* **1983**, *28*, 1207−1209.

(16) Grin, Y.; Yarmolyuk, Y. P.; Rozhdestvenskaya, I. V.; Gladyshevskii, E. I. Crystal Chemistry of a Series of Inhomogeneous Linear Structures with the Crystal Structure of $LaGa_6Ni_{(1-x)}$ and $CeGa_6Ni_{(1-x)}$. *Kristallografiya* **1982**, *27*, 418−419.

(17) Grin, Y.; Rozhdestvenskaya, I. V.; Usov, O. A.; Kuz'min, A. M.; Bruskov, V. A.; Gladyshevskii, E. I. Crystal Chemistry of Series of Inhomogeneous Linear Structures 3. The Crystal Structures of $Ce_2Ga_{10}Ni$ and $La_2Ga_{10}Ni$. *Kristallografiya* **1982**, *27*, 999−1001.

(18) Grin, Y.; Yarmolyuk, Y. P.; Zavodnik, V. E. Crystal Chemistry of a Series of Inhomogeneous Linear Structures. The Crystal Stucture of the Compound $Ce_3Ga_{15}Ni_2$. *Kristallografiya* **1984**, *29*, 228−231.

(19) Cava, R. J.; Ramirez, A. P.; Takagi, H.; Krajewski, J. J.; Peck, W. F. Physical Properties of Some Ternary Ce Intermetallics with the Transition Metals Ni and Pd. *J. Magn. Magn. Mater.* **1993**, 124−128.

(20) Grin, Y. N.; Hiebl, K.; Rogl, P.; Noël, H. Magnetism and Structural Chemistry of Ternary Gallides $RENi_xGa_{4-x}$ and $LaCo_0$. *J. Less-Common Metals, 5Ga3.5* **1990**, *162*, 361−369.

(21) Sheldrick, G. M. *SHELXTL NT/2000, Version 6.1*; Bruker AXS, Inc.: Madison, WI, 2000
(22) Hübschle, C. B.; Sheldrick, G. M.; Dittrich, B. ShelXle: a Qt graphical user interface for SHELXL. *J. Appl. Crystallogr.* **2011**, *44*, 1281−1284.
(23) Huq, A.; Hodges, J. P.; Gourdon, O. A.; Heroux, L. POWGEN: A Third-Generation High Resolution High-Throughput Powder Diffraction Instrument at the Spallation Neutron Source. *Z. Kristallogr.* **2011**, *1*, 127−135.
(24) Peterson, P. F.; Campbell, S. I.; Reuter, M. A.; Taylor, R. J.; Zikovsky, J. Event-Based Processing of Neutron Scattering Data. *Nucl. Instrum. Methods Phys. Res., Sect. A* **2015**, *803*, 24−28.
(25) Jepsen, O.; Burkhardt, A.; Andersen, O. K. *The Program TB-LMTO-ASA, version 4.7*; Max-Planck Institut fur Festkorperforschung: Stuttgart, Germany, 2000.
(26) Blöchl, P. E.; Jepsen, O.; Andersen, O. K. Improved Tetrahedron Method for Brillouin-zone Integrations. *Phys. Rev. B* **1994**, *49*, 16223−16233.
(27) Stewart, G. R.; et al. *Rev. Mod. Phys.* **1984**, *56*, 755.
(28) Moshopoulou, E. G.; Sarrao, J. L.; Pagliuso, P. G.; Moreno, N. O.; Thompson, J. D.; Fisk, Z.; Ibberson, R. M. Comparison of the Crystal Structure of the Heavy-fermion Materials $CeCoIn_5$, $CeRhIn_5$ and $CeIrIn_5$. *Appl. Phys. A: Mater. Sci. Process.* **2002**, *74*, s895−s897.
(29) Kratochvilova, M.; Dusek, M.; Uhlirova, K.; Rudajevova, A.; Prokleska, J.; Vondrackova, B.; Custers, J.; Sechovsky, V. Single Crystal Study of the Layered Heavy Fermion Compounds Ce_2PdIn_8, Ce_3PdIn_{11},Ce_2PtIn_8 and Ce_3PtIn_{11}. *J. Cryst. Growth* **2014**, *397*, 47−52.
(30) Pfleiderer, C. Superconducting Phases of *f*-electron Compounds. *Rev. Mod. Phys.* **2009**, *81*, 1551.
(31) Hafner, D.; Rai, B. K.; Banda, J.; Kliemt, K.; Krellner, C.; Sichelschmidt, J.; Morosan, E.; Geibel, C.; Brando, M. Kondo-lattice Ferromagnets and their Peculiar Order Along the Magnetically Hard Axis Determined by the Crystalline Electric Field. *Phys. Rev. B* **2019**, *99*, 201109.
(32) Lai, Y.; Bone, S. E.; Minasian, S.; Ferrier, M. G.; Lezama-Pacheco, J.; Mocko, V.; Ditter, A. S.; Kozimor, S. A.; Seidler, G. T.; Nelson, W. L.; Chiu, Y.-C.; Huang, K.; Potter, W.; Graf, D.; Albrecht-Schmitt, T. E.; Baumbach, R. E. Ferromagnetic Quantum Critical Point in $CePd_2P_2$ with Pd → Ni Substitution. *Phys. Rev. B* **2018**, *97*, 224406.
(33) Baumbach, R. E.; Shang, T.; Torrez, M.; Ronning, F.; Thompson, J. D.; Bauer, E. D. Local Moment Ferromagnetism in $CeRu_2Ga_2B$. *J. Phys.: Condens. Matter* **2012**, *24*, No. 085702.

https://doi.org/10.1021/acs.inorgchem.2c02588
Inorg. Chem. XXXX, XXX, XXX−XXX